Applied Physics Letters

Near-field thermophotonic system for power generation and electroluminescent refrigeration

Cite as: Appl. Phys. Lett. **120**, 053902 (2022); https://doi.org/10.1063/5.0076765
Submitted: 27 October 2021 • Accepted: 23 January 2022 • Published Online: 04 February 2022

Fan Yang, Kaifeng Chen, Yiting Zhao, et al.

Applied Physics Letters ARTICLE scitation.org/journal/apl

Near-field thermophotonic system for power generation and electroluminescent refrigeration

Cite as: Appl. Phys. Lett. **120**, 053902 (2022); doi: 10.1063/5.0076765
Submitted: 27 October 2021 · Accepted: 23 January 2022 ·
Published Online: 4 February 2022

Fan Yang,[1] Kaifeng Chen,[2] Yiting Zhao,[1] Sun-Kyung Kim,[3] Xiaobing Luo,[1,4] and Run Hu[1,4,5,a)]

AFFILIATIONS

[1]China-EU Institute for Clean and Renewable Energy, Huazhong University of Science and Technology, Wuhan 430074, China
[2]Department of Applied Physics, Stanford University, Stanford, California 94305, USA
[3]Department of Applied Physics, Kyung Hee University, 1732 Deogyeong-daero, Giheung-gu, Yongin-Si, Gyeonggi-do 446-701, Republic of Korea
[4]School of Energy and Power Engineering, Huazhong University of Science and Technology, Wuhan 430074, China
[5]Wuhan National Laboratory for Optoelectronics, Huazhong University of Science and Technology, Wuhan 430074, China

[a)]Author to whom correspondence should be addressed: hurun@hust.edu.cn

ABSTRACT

Near-field thermophotonic (TPX) systems that replace the high-temperature emitter in the thermophotovoltaic systems with a light-emitting diode (LED) have been reported to achieve low-grade heat harvesting and electroluminescent cooling, respectively. Nevertheless, the requirements for the two functionalities are different, leading to challenges to coordinate them. In our work, we propose a near-field TPX system composed of the CdTe LED and InP photovoltaic (PV) cell to realize two such functionalities with high performance. With wide-bandgap and high-quality semiconductors, the proposed system achieves a bandgap alignment at various temperatures and has low nonradiative recombination rates, thus enabling the functionality integration. Without changing the structures and materials, the system can switch functionality from power generation to electroluminescent refrigeration by tuning the LED temperature from 800 to 260 K while the PV temperature is maintained at 300 K. In addition, we suggest an additional layer of a thin Pt film on the PV cell to suppress phonon-polaritons parasitic heat transfer and further improve the system efficiency of both functionalities. This work theoretically demonstrates the possible integration of multiple functionalities and triggers further explorations of practical TPX systems.

Near-field heat transfer has been theoretically and experimentally proven to significantly exceed the limit of blackbody radiation as the evanescent waves dominate and enhance the heat transfer in near-field regime.[1,2] The theory was first predicted by Polder and Van Hove in 1971[2] and was then experimentally validated in different configurations and materials.[3–5] Because of such enhancement, the near-field heat transfer system has been widely used in many energy-related devices, for example, near-field thermophotovoltaics (NF-TPVs).[6–10] In a NF-TPV system, a specially designed thermal emitter is separated to a photovoltaic (PV) cell with a nanoscale gap to convert the thermal radiation from the emitter into electricity.[11–13] The NF-TPV system originates from the far-field TPV systems, and the main difference is the nanoscale gap between the thermal emitter and the PV cell.[14] Due to the near-field effect, the NF-TPV systems are able to offer higher electrical power generation (EPG) than their far-field counterpart. Since only the emitted photons above the bandgap can be absorbed by the PV cell for power generation, it is natural to elevate the temperature of the emitter above 1000 K so as to shift the photon distribution toward the bandgap of the PV cell.[15] However, the thermal energy with the temperature below 1000 K is common and massive, and thus, harvesting such a low-grade energy is of great significance.

To this end, a similar near-field heat transfer system called near-field thermophotonics (NF-TPX) is proposed, where the thermal emitter of the NF-TPV system is replaced by a light-emitting diode (LED).[16] By this means, the broad-spectrum thermal radiation is replaced with a narrow-spectrum electroluminescence around the bandgap of the LED. Both thermal radiation and the electroluminescence from the LED can be utilized for the energy conversion via electrical control and wave tunneling.[17] The NF-TPX system outputs power when the generated power is more than the power consumed by the LED. For example, a NF-TPX system consisting of a 600 K $Al_{0.32}Ga_{0.68}As$ LED and a 300 K $Al_{0.155}Ga_{0.845}As$ PV cell was reported to reach a maximum EPG of 9.58 W/cm^2 or the maximum efficiency

of 9.76%, corresponding to a ZT of 0.86.[16] In such a NF-TPX system, the bandgaps of the LED and PV cell are suggested to be aligned due to the coupling of materials and the working temperature, and even a small misalignment of 0.05 eV can degrade the maximum EPG to 0.63 W/cm^2.

Not only for EPG, such a NF-TPX system can also be used for electroluminescent refrigeration (ELR).[18] To achieve ELR, the LED works as the cold reservoir while the PV cell works as the hot reservoir. With light as the working fluid, heat is pumped from a cold LED to a hot PV cell. It was reported that the maximum cooling power of a NF-TPX system, consisting of a GaAs LED and a Si PV cell, reached the magnitude of 10 W/cm^2 and the maximum coefficient of performance (COP) of the system was 10% of the Carnot limit.[19] To achieve high-performance ELR, a LED with high quantum efficiency is desired.[17,20] In addition, phonon polaritons also hinder ELR, in particular for a system made of polarized semiconductor materials.[19] Since phonon polaritons have frequencies lower than the bandgap of the semiconductor, such sub-bandgap radiation induced by the phonon polaritons cannot be used for power generation, thus leading to significant refrigeration leakage where heat transfer occurs from hot side to cool side. Therefore, effective measures against phonon polaritons are also expected to be introduced for ELR.

Reviewing aforementioned works, the requirements for EPG and ELR functionalities are different, thus leaving challenges to achieve them simultaneously. In this work, we design a NF-TPX system shown in Fig. 1, which can be used for both EPG and ELR functionalities. The system configuration consists of a CdTe LED and an InP PV cell with both backed by perfect electric conductor mirrors. Their wide-bandgap structures provide possibilities to match a bandgap alignment at various temperatures for EPG, and their low nonradiative recombination rates induce feasibility for ELR. To further improve the performance, a thin platinum (Pt) film is added on top of the PV cell to repress the parasitic heat transfer occurring below the bandgap. In implementation, we tune LED temperature to switch functionality from EPG to ELR, while the PV cell temperature is maintained at 300 K by an external heat sink. For the EPG functionality, the LED works as the hot reservoir with a temperature above 300 K, shown in Fig. 1(a). The LED is driven by part of output power generated from the PV cell, and the rest energy serves as the net output. As the temperature of the LED decreases below 300 K, EPG vanishes and the system works in the ELR functionality, shown as Fig. 1(b). The LED is driven by an external input power, part of which is supplied from the PV cell. In this scenario, the LED emits photons with higher energy than that of the PV cell to refrigerate the cool source.

We study the near-field heat transfer system with the formalism of fluctuational electrodynamics, which yields the energy flux of electronic excitations E^{e} above the bandgap, and the parasitic sub-bandgap heat transfer due to the phonon-polaritons excitations E^{p} with the following equations:[2,18]

$$E^{\mathrm{e}}_{a\to b} = \int_{\omega_{\mathrm{th}}}^{+\infty} \Theta(\omega, T_a, V_a)\Phi(\omega)d\omega, \tag{1}$$

$$E^{\mathrm{p}}_{a\to b} = \int_{0}^{\omega_{\mathrm{th}}} \Theta(\omega, T_a, 0)\Phi(\omega)d\omega, \tag{2}$$

where subscript $a \to b$ denotes the flux, which is emitted by object a and reaches object b. ω_{th} is the threshold frequency, which is the maximum of the bandgap frequency between LED and PV, i.e., $\omega_{\mathrm{th}} = \max(\omega_{\mathrm{g1}}, \omega_{\mathrm{g2}})$, where subscripts 1 and 2 represent the LED and PV cell, respectively. Assuming the materials are lossless and the existence of perfect electric conductor mirrors, we model the photons exchange that only occurs above ω_{th}, as shown in Eq. (1). The contributions of both the propagating and evanescent waves are included in Eqs. (1) and (2). $\Theta(\omega, T, V)$ is the expectation value of the photon energy in a single mode at angular frequency ω, as

$$\Theta(\omega, T, V) = \frac{\hbar\omega}{\exp\left(\frac{\hbar\omega - qV}{k_{\mathrm{B}}T}\right) - 1}, \tag{3}$$

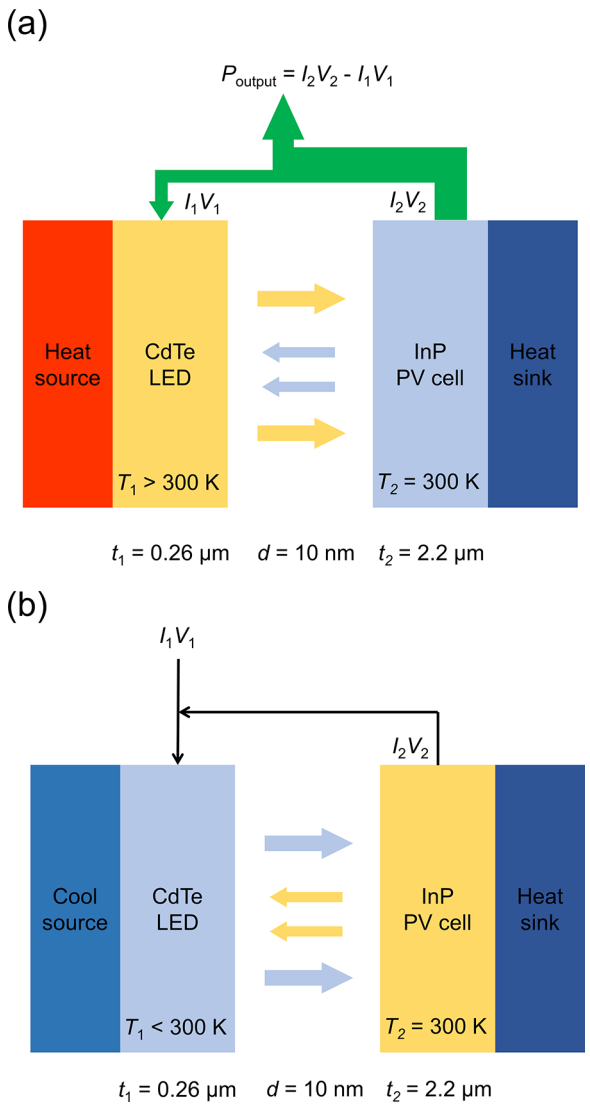

FIG. 1. Schematic of the NF-TPX system working at different temperatures in EPG and ELR functionalities. The LED is made of CdTe, and the PV cell is made of InP. (a) Diagram for EPG functionality: the LED consumes energy from the heat source for electricity generation, driven by the radiation from the PV cell. (b) Diagram for ELR functionality: the LED emits more energy than the PV cell to refrigerate the cool source, powered by an external input.

where q is the magnitude of the electron charge, $\hbar$ is the reduced Planck's constant, k_B is the Boltzmann constant, and V is the voltage on the studied object. $\Phi(\omega)$ in Eqs. (1) and (2) is the energy transfer coefficient and can be calculated with the standard dyadic Green's function and scattering matrix method,[2,16,21–23] and it is formulated as follows:

$$\Phi(\omega) = \frac{1}{4\pi^2}\int_0^{\infty} \xi(\omega, k_{\parallel})\mathrm{k}_{\parallel} dk_{\parallel}, \tag{4}$$

where ξ is the energy transmission coefficient and $k_{||}$ is the parallel component of the wavevector. In addition, the voltage of the LED should be lower than $(\hbar\omega_g/q)$ for the formalism to be valid. The dielectric functions of CdTe and InP are obtained from Ref. 24, and the bandgaps of them are calculated from Refs. 25 and 26.

Therefore, the photon flux calculation can be yielded as

$$F_{a\to b} = \int_{\omega_{\mathrm{th}}}^{+\infty} \frac{\Theta(\omega, T_a, V_a)}{\hbar\omega}\Phi(\omega)d\omega, \tag{5}$$

and the current density in both the LED and the PV cell can be calculated as

$$I_1 = q(F_{1\to 2} - F_{2\to 1} + R_1), \tag{6}$$

$$I_2 = q(F_{1\to 2} - F_{2\to 1} - R_2), \tag{7}$$

where R represents the net nonradiative recombination.

The nonradiative recombination includes Auger and Shockley–Read–Hall (SRH) recombinations, and they are given as[16,19]

$$R = R_{\mathrm{Auger}} + R_{\mathrm{SRH}} = (C_n n + C_p p)(np - n_i^2)t + \frac{(np - n_i^2)t}{\tau(n + p + 2n_i)}, \tag{8}$$

where n, p, and n_i are the electron concentration, hole concentration, and intrinsic carrier concentration, respectively. C_n and C_p are the Auger coefficients. t is the thickness of the LED or PV cell, and τ is the SRH lifetime. We assume that the Auger recombination coefficient of CdTe is 2×10^{-32} cm^6/s and that of InP is 9×10^{-31} cm^6/s.[20,25,27,28] The intrinsic carrier concentration of CdTe is calculated as from 1.3×10^6 to 2×10^{15} cm^{-3}, corresponding to the temperature from 300 to 800 K[26] and that of InP is 1.2×10^7 cm^{-3} at 300 K.[25] The lifetime is assumed to be 1 s in semi-insulating bulk CdTe grown from the melt range[29,30] and that of InP is 10 μs.[31] Since the optimal operation voltage of CdTe is at around 1 V and that of InP is at around 1.2 V, which will be discussed later, Auger and SRH recombinations are compared under each optimal operation condition. For CdTe working from 300 to 800 K, the ratio of $R_{\mathrm{Auger}}/R_{\mathrm{SRH}}$ is calculated to be 6.3×10^3 and 5.7×10^4, respectively. Therefore, we assume that the SRH recombination in CdTe is negligible compared to Auger recombination. For InP maintained at 300 K, the ratio of $R_{\mathrm{Auger}}/R_{\mathrm{SRH}}$ is 10. However, since the photon flux from LED is much higher than nonradiative recombination, such a 10% difference seldom interferes with the generated current, according to Eq. (7). Therefore, in the following discussions, only the Auger recombination is considered.[18,19]

Considering the relation between nonradiative recombination and thickness, the system performance partly depends on the thickness. We vary the thickness from 0.1 to 5 μm to locate the optimal range under EPG and ELR. The best value of LED thickness approximates to 0.2 μm and that of the PV cell is around 2 μm. Therefore, we choose the thicknesses as 0.26 and 2.2 μm, respectively, which works the best for EPG and barely interferes with the ELR. Consequently, the net energy flux of LED is inferred as

$$Q = \left(E^{\mathrm{e}}_{1\to 2} + E^{\mathrm{p}}_{1\to 2}\right) - \left(E^{\mathrm{e}}_{2\to 1} + E^{\mathrm{p}}_{2\to 1}\right) - I_1 V_1. \tag{9a}$$

When the Pt film is covered, the net energy flux of the LED is yielded as

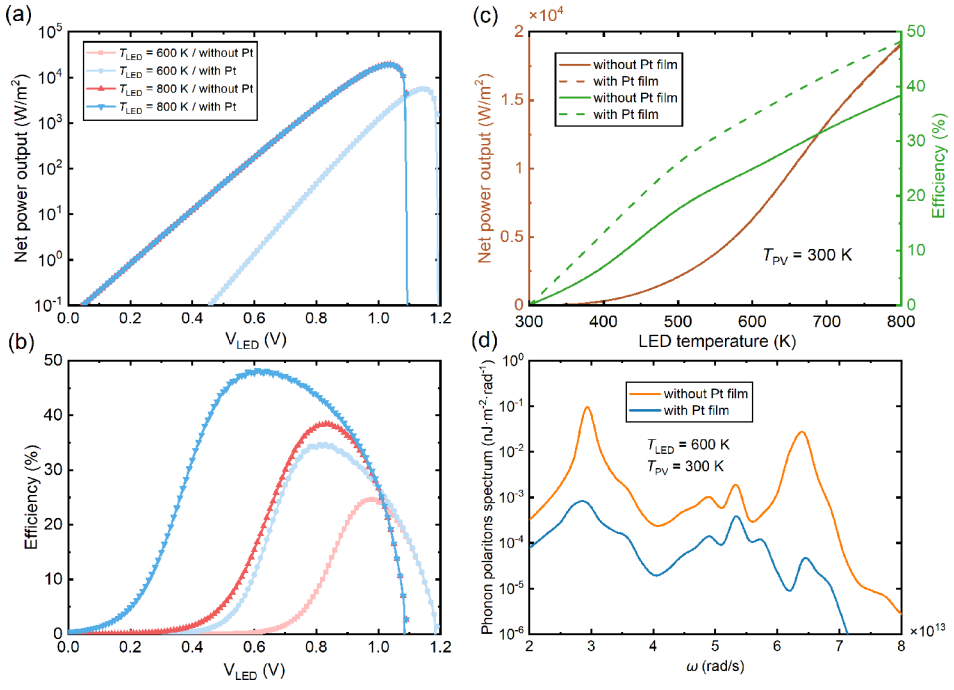

FIG. 2. Net power output (a) and efficiencies (b) of EPG at temperatures of 600 and 800 K. (c) Maximum power and maximum efficiency at the corresponding optimal applied voltage with and without the Pt film. LED temperature increases from 300 K, while the temperature of the PV cell is maintained at 300 K. (d) Effect of the Pt film on the suppression of phonon-polaritons heat transfer below the bandgap.

$$Q = \left(E^{e}_{1\to Pt} + E^{p}_{1\to Pt}\right) - \left(E^{e}_{2\to 1} + E^{p}_{2\to 1} + E^{e}_{Pt\to 1} + E^{p}_{Pt\to 1}\right) - I_1 V_1, \tag{9b}$$

where the first two terms ($E^{e}_{1\to Pt}$, $E^{p}_{1\to Pt}$) represent the total energy flux emitted from LED and the successive four terms ($E^{e}_{2\to 1}$, $E^{p}_{2\to 1}$, $E^{e}_{Pt\to 1}$, $E^{p}_{Pt\to 1}$) represent the total energy flux reaching the LED, respectively. We first study the EPG functionality and decrease the temperature of LED from 800 to 300 K, while maintaining the PV cell at 300 K. The energy is ejected from the LED to the PV cell, and part of the power generated by PV cell is fed back to LED. We tune the voltage of PV cell for the maximum power output. Hence, the net power is formulated as

$$P = I_2 V_2 - I_1 V_1, \tag{10}$$

and the system efficiency is defined as

$$\eta = \frac{P}{Q}. \tag{11}$$

The net power and efficiency of the present NF-TPX system are shown in Fig. 2. In general, the photon flux emitted from the LED increases with applied voltage, thus resulting in higher power and efficiency. From Eqs. (6) and (7), the current density of the LED is higher than that of the PV cell, thus requesting the voltage of the PV cell should be higher than that of the LED in order to achieve net power output. Nevertheless, exceedingly high voltage on the LED or PV cell will cause the increase in carrier density and nonradiative recombination rate, which overwhelms the radiative recombination rate and thus drastically degrades the power and efficiency. Therefore, along with the increase in LED voltage, there exist peaks on both power and efficiency curves in Figs. 2(a) and 2(b). We also note that the peaks of power and efficiency shift toward lower voltage with the increase in LED temperature, and it can be interpreted as effective temperature by[32,33]

$$\Theta(\omega, T, V) = \frac{\hbar\omega}{\exp\left(\frac{\hbar\omega - qV}{k_B T}\right) - 1} = \frac{\hbar\omega}{\exp\left(\frac{\hbar\omega}{k_B T^*}\right) - 1}. \tag{12}$$

From Eq. (12), the increasing effective temperature (T^*) is concerned as additional voltage (V), which, in turn, reduces the factual need of applied voltage.

We note that the maximum power or efficiency occurs at different applied voltages, so one may tune the voltage to meet requirements of power or efficiency. The maximum power or efficiency at various temperatures are plotted in Fig. 2(c). It is seen that both the power and efficiency increase when LED temperature increases. When the LED temperature is tuned below 400 K, the radiative recombination is small compared to the nonradiative recombination, and hence, power and efficiency become negligible. With an ascending LED temperature, power and efficiency improve due to the increased emission ability according to Eq. (3). Therefore, the best performance occurs at the temperature of 800 K, and the maximum net power generation of

TABLE I. The comparison of system efficiencies with and without the Pt film. The applied voltage of the LED is controlled at 1 V ($V_{LED} = 1$ V).

	Without Pt film	With Pt film
400 K	3.37%	12.28%
600 K	24.16%	26.63%
800 K	26.63%	26.93%

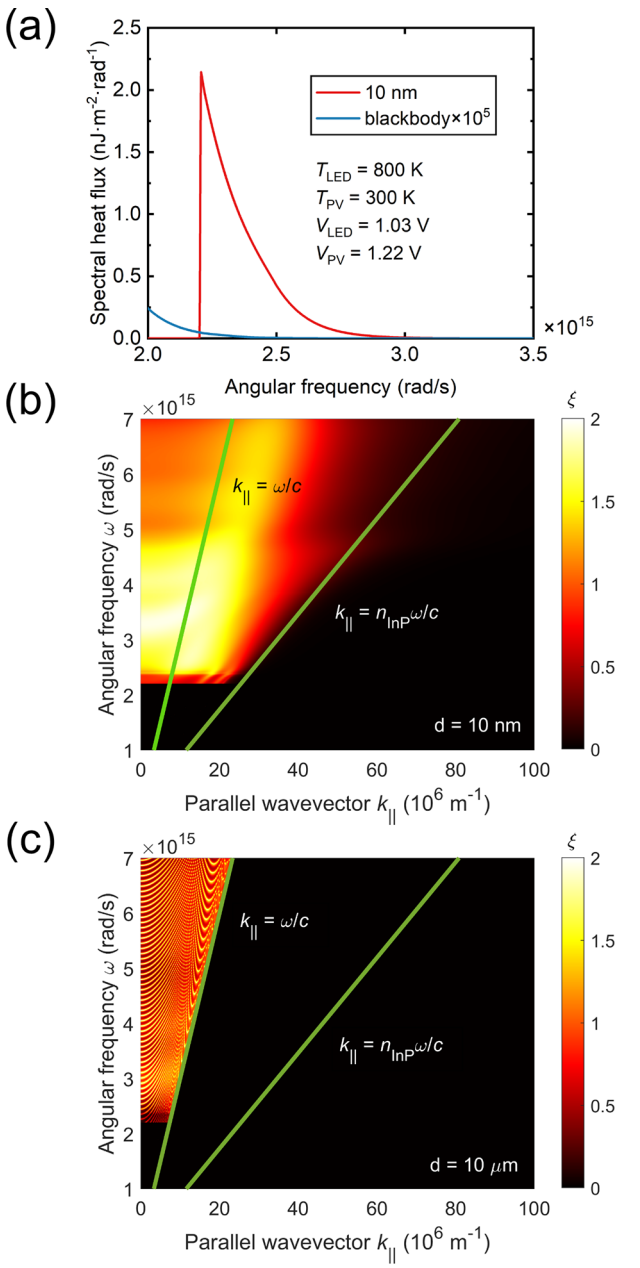

FIG. 3. (a) Above-bandgap spectral heat flux between the LED and the PV cell for the system with the vacuum gap of 10 nm, which is 10^5 higher in magnitude than the blackbody radiation. (b) Energy transmission coefficient between the LED and PV cell as a function of frequency and parallel wavevector for the system. The green lines are the light lines of vacuum and InP with a refractive index $n_{InP} = 3.4$, and c is the speed of light in vacuum. The vacuum gap between the LED and PV cell is 10 nm. (c) Energy transmission coefficient when the vacuum gap is 10 μm, referring to the far-field regime.

1.91×10^4 W/m^2 or the maximum efficiency of 48.2% are found. Such high-performance efficiency makes low-grade waste heat recovery possible and efficient.

To improve the efficiency of system, we employ the method following Ref. 34 to suppress the sub-bandgap heat transfer due to phonon polaritons, and a Pt film of 2 nm is attached to the PV cell. The dielectric function of Pt is calculated based on the Drude model $\varepsilon(\omega) = \varepsilon_\infty - \omega_p^2/(\omega^2 + i\omega\Gamma)$, where $\varepsilon_\infty = 5.4$, $\omega_p = 5.145$ eV, and $\Gamma = 0.0169$ eV.[34,35] The Pt film enhances the system efficiency significantly, while making a little reduction on the net EPG as is illustrated in Figs. 2(a)–2(c). In addition, Table I illustrates the improvement after Pt is covered. At a fixed applied voltage, the Pt film helps in improving the system efficiency at various temperatures and the larger enhancement effect occurs at lower temperature. To further understand the suppression of phonon polaritons by the Pt film, we plot the power spectrum as a function of frequency below the bandgap in Fig. 2(d). The peak of sub-bandgap heat transfer drops two orders of magnitude because of the Pt film, compared with the original system. Pt shows high values of the imaginary part of the dielectric function at low frequency, thus inducing significant loss for radiative transfer that, in turn, suppresses sub-bandgap heat transfer due to the phonon polaritons. We note that other alternative noble metal films, such as Ag and W, can play the same role.[35,36]

The enhanced heat transfer can be further understood through Fig. 3(a). Compared to the far-field blackbody spectrum, the spectral heat flux of the near-field regime is significantly enhanced, and it can be interpreted by subsequent figures. Figure 3(b) shows the energy transmission coefficient as a function of frequency and the parallel wavevector. We observe energy transmission between two light lines of vacuum and InP, revealing significant contribution of evanescent wave tunneling to the heat transfer. However, the energy transmission only occurs above the light line of vacuum in the far-field regime, as is shown in Fig. 3(c). Therefore, the near-field heat transfer is enhanced due to the evanescent wave tunneling between the LED and the PV cell.

We further lower the LED temperature under 300 K, and the system can work for ELR as shown in Fig. 1(b). Specifically, the PV cell temperature is still maintained at 300 K through the heat sink, and we tune the LED temperature from 300 to 260 K. The intrinsic carrier concentration of InP is calculated as 1.2×10^7 cm^{-3} and that of CdTe varies from 1.3×10^6at 300 to 8.4×10^3 cm^{-3} at 260 K.[25,26] The cooling power can also be quantified by Eq. (9), and the coefficient of performance (COP) is defined as

$$COP = \frac{Q}{I_1 V_1 - I_2 V_2}. \tag{13}$$

As the operation temperature is tuned below 300 K, phonon-polaritons heat transfer plays a more negative role on ELR, since the radiative recombination rate decreases at lower temperature. We take the case of a 280 K LED for analysis, and the results are shown in Figs. 4(a) and 4(b). Working for the ELR functionality, the system reaches the maximum cooling power of 3.05×10^5 W/m^2 or the maximum COP of 34.26% (normalized to Carnot efficiency, i.e., 14 at this temperature difference), which is equal to a thermoelectric refrigerator with a ZT of 3.6. In the absence of the Pt film, as shown in Figs. 4(a) and 4(b), the phonon-polaritons heat transfer undermines the cooling power and COP at low applied voltages. Therefore, ELR only works within a narrow range of applied voltage. When the Pt film is covered, the phonon-polaritons heat transfer is significantly suppressed as is shown in Fig. 4(c). Continuously tuning the temperature of the LED, we pick the maximum cooling power or efficiency at corresponding temperature and plot Fig. 4(d). As the temperature decreases, the

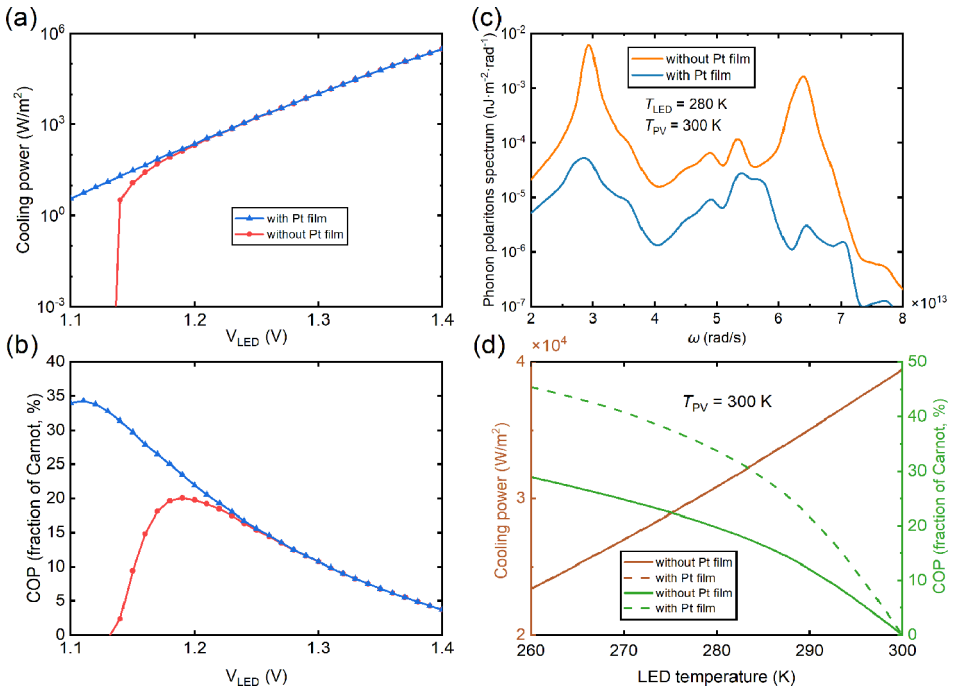

FIG. 4. Cooling power (a) and COP normalized to the Carnot limit (b) as a function of applied voltage on the LED. Phonon polaritons severely impact cooling power and COP at low applied voltage, while the Pt film can suppress such sub-bandgap heat transfer. (c) Effect of the Pt film on the suppression of sub-bandgap heat transfer. (d) Maximum cooling power and maximum COP from 260 to 300 K.

cooling power is reduced due to the reduced emitting ability. With the elevated temperature, COP is decreasing at the expense of higher power input, and the corresponding Carnot limit approaches infinity. It may be counterintuitive to refrigerate when the LED temperature is equal to that of the PV cell, i.e., 300 K. However, considering Eq. (12), where the thermodynamic temperature (T) is considered as effective temperature (T^*) and the latter is actually higher than the former, it makes sense that the refrigerator still works with a very little COP.

In conclusion, we proposed an effective near-field thermophotonics (NF-TPX) system for electric power generation (EPG) from low-temperature waste heat and electroluminescent refrigeration (ELR) without changing the structures and materials. For EPG, driven by part of the electric power from the PV cell, the LED emits photons to the PV cell, and the system reaches high power and efficiency even at low temperature. For ELR, the LED ejects energy flux driven by an external power input, which is partly supplied from the PV cell. The efficiency of both functionalities can be improved by adding a thin layer of Pt film on top of the PV cell to suppress sub-bandgap heat transfer induced by phonon polaritons. We may use the ELR functionality for the cooling process and use the EPG functionality for waste heat recovery during the implementation of the system. Our work proposes a NF-TPX system simultaneously fulfilling EPG and ELR without necessarily changing configuration or materials and points to the theoretical possibilities of the near-field heat transfer system working for various purposes and temperatures.

The authors acknowledge the financial support from the Open Project Program of Wuhan National Laboratory for Optoelectronics (No. 2021WNLOKF004), the National Natural Science Foundation of China (No. 52076087), and the Wuhan City Science and Technology Program (No. 2020010601012197).

AUTHOR DECLARATIONS

Conflict of Interest

The authors have no conflicts to disclose.

DATA AVAILABILITY

The data that support the findings of this study are available from the corresponding author upon reasonable request.

REFERENCES

[1]J. J. Loomis and H. J. Maris, Phys. Rev. B **50**, 18517 (1994).
[2]D. Polder and M. Van Hove, Phys. Rev. B **4**, 3303 (1971).
[3]Z. M. Zhang, *Nano/Microscale Heat Transfer* (Springer International Publishing, Cham, 2020).
[4]S.-A. Biehs, R. Messina, P. S. Venkataram, A. W. Rodriguez, J. C. Cuevas, and P. Ben-Abdallah, Rev. Mod. Phys. **93**, 025009 (2021).
[5]M. Ghashami, A. Jarzembski, M. Lim, B. J. Lee, and K. Park, Annu. Rev. Heat Transfer **23**, 13 (2020).
[6]W. A. Callahan, D. Feng, Z. M. Zhang, E. S. Toberer, A. J. Ferguson, and E. J. Tervo, Phys. Rev. Appl. **15**, 054035 (2021).
[7]D. Fan, T. Burger, S. McSherry, B. Lee, A. Lenert, and S. R. Forrest, Nature **586**, 237 (2020).
[8]A. Fiorino, L. Zhu, D. Thompson, R. Mittapally, P. Reddy, and E. Meyhofer, Nat. Nanotechnol. **13**, 806 (2018).
[9]K. Park, S. Basu, W. P. King, and Z. M. Zhang, J. Quant. Spectrosc. Radiat. Transfer **109**, 305 (2008).
[10]K. Li, S. Wu, S. Cao, Q. Cai, Q. Ye, X. Liu, and X. Wu, Appl. Therm. Eng. **192**, 116918 (2021).
[11]N.-P. Harder and P. Würfel, Semicond. Sci. Technol. **18**, S151 (2003).
[12]J. Song, Q. Cheng, B. Zhang, L. Lu, X. Zhou, Z. Luo, and R. Hu, Rep. Prog. Phys. **84**, 036501 (2021).
[13]J. Song, L. Lu, B. Li, B. Zhang, R. Hu, X. Zhou, and Q. Cheng, Int. J. Heat Mass Transfer **150**, 119346 (2020).
[14]R. Hu, J. Song, Y. Liu, W. Xi, Y. Zhao, X. Yu, Q. Cheng, G. Tao, and X. Luo, Nano Energy **72**, 104687 (2020).
[15]M. M. A. Gamel, H. J. Lee, W. E. S. W. A. Rashid, P. J. Ker, L. K. Yau, M. A. Hannan, and M. Z. Jamaludin, Materials **14**, 4944 (2021).
[16]B. Zhao, P. Santhanam, K. Chen, S. Buddhiraju, and S. Fan, Nano Lett. **18**, 5224 (2018).
[17]T. Sadi, I. Radevici, and J. Oksanen, Nat. Photonics **14**, 205 (2020).
[18]K. Chen, P. Santhanam, S. Sandhu, L. Zhu, and S. Fan, Phys. Rev. B **91**, 134301 (2015).
[19]K. Chen, T. P. Xiao, P. Santhanam, E. Yablonovitch, and S. Fan, J. Appl. Phys. **122**, 143104 (2017).
[20]K. A. Bulashevich and S. Yu. Karpov, Phys. Status Solidi C **5**, 2066 (2008).
[21]K. Chen, B. Zhao, and S. Fan, Comput. Phys. Commun. **231**, 163 (2018).
[22]D. M. Whittaker and I. S. Culshaw, Phys. Rev. B **60**, 2610 (1999).
[23]D. Feng, E. J. Tervo, D. Vasileska, S. K. Yee, A. Rohatgi, and Z. M. Zhang, J. Appl. Phys. **129**, 213101 (2021).
[24]E. Palik, *Handbook of Optical Constants of Solids* (Academic, New York, 1985).
[25]I. P.-T. Institute, *NSM Archive-Physical Properties of Semiconductors* (I. P.-T. Institute, 1998).
[26]C.-H. Su, J. Appl. Phys. **103**, 084903 (2008).
[27]H. Wen, B. Pinkie, and E. Bellotti, J. Appl. Phys. **118**, 015702 (2015).
[28]P. Ščajev, S. Miasojedovas, A. Mekys, D. Kuciauskas, K. G. Lynn, S. K. Swain, and K. Jarašiūnas, J. Appl. Phys. **123**, 025704 (2018).
[29]C. Buurma, S. Krishnamurthy, and S. Sivananthan, J. Appl. Phys. **116**, 013102 (2014).
[30]C. J. Johnson, E. E. Eissler, S. E. Cameron, Y. Kong, S. Fan, S. Jovanovic, and K. G. Lynn, MRS Proc. **302**, 463 (1993).
[31]A. Liu and Y. Rosenwaks, J. Appl. Phys. **86**, 430 (1999).
[32]K. Chen, P. Santhanam, and S. Fan, Phys. Rev. Appl. **6**, 024014 (2016).
[33]E. Tervo, E. Bagherisereshki, and Z. Zhang, Front. Energy **12**, 5 (2018).
[34]B. Zhao, K. Chen, S. Buddhiraju, G. Bhatt, M. Lipson, and S. Fan, Nano Energy **41**, 344 (2017).
[35]H. Gai, J. Wang, and Q. Tian, Appl. Opt. **46**, 2229 (2007).
[36]M. A. Ordal, R. J. Bell, R. W. Alexander, L. L. Long, and M. R. Querry, Appl. Opt. **24**, 4493 (1985).